Spin–orbit branching in the photodissociation of HF and DF. I. A time-dependent wave packet study for excitation from $v=0$

Alex Brown[a] and Gabriel G. Balint-Kurti[b]
School of Chemistry, University of Bristol, Bristol BS8 1TS, United Kingdom

(Received 15 March 2000; accepted 4 May 2000)

The photodissociation dynamics of HF and DF, following $A\,^1\Pi \leftarrow X\,^1\Sigma^+$ electronic excitation, are examined using time-dependent wave packet techniques. The calculations are based on new multireference configuration interaction calculations of the potential energy curves and complete active space self-consistent field calculations of the off-diagonal spin–orbit coupling matrix elements. The calculated branching fraction for the formation of excited state fluorine, $F^*(^2P_{1/2})$, following excitation from the ground vibrational state ($v=0$) of HF, agrees well with the value of 0.41 ± 0.08 measured experimentally at 121.6 nm by Zhang *et al.* [J. Chem. Phys. **104**, 7027 (1996)]. Predictions are made for the excited spin–orbit state branching fraction for both HF and DF over a wide range of photon excitation energies. The results for HF and DF are discussed in context with the corresponding results for the photodissociation of HCl and DCl. © *2000 American Institute of Physics.* [S0021-9606(00)01529-4]

I. INTRODUCTION

The hydrogen halides (HX, X=F, Cl, Br, I), and the corresponding deuterated species, provide model systems for studying molecular photodissociation dynamics on multiple coupled potential energy curves (PECs). The photodissociation process involves two inter-connected processes: (i) initial excitation to one (or more) of the PECs, and (ii) nonadiabatic transitions between the excited PECs as the molecule fragments. The roles of these two processes can be investigated experimentally by measuring the relative contributions of the two spin–orbit states which can be produced from this photodissociation process,

$$\begin{aligned} HX + h\nu &\rightarrow H(^2S) + X(^2P_{3/2}) \\ &\rightarrow H(^2S) + X(^2P_{1/2}), \end{aligned} \tag{1}$$

and the photofragment angular distributions. Using the customary nomenclature, the halogen atom spin–orbit states are designated as X and X^* for $X(^2P_{3/2})$ and $X(^2P_{1/2})$, respectively.

Neglecting spin–orbit coupling, four electronic states, $^1\Sigma^+$, $^1\Pi$, $^3\Pi$, and $^3\Sigma^+$, correlate with the lowest energy asymptote, $H(^2S)+X(^2P)$. Only the $X\,^1\Sigma^+$ state is bound for the hydrogen halide molecules. The photodissociation occurs after initial excitation to the $^1\Pi_{\Omega=1}$, $^3\Pi_1$, $^3\Pi_0$, and $^3\Sigma_1^+$ states. When the spin–orbit constant in the halogen atom is small, i.e., F or Cl, the initial excitation primarily occurs from the bound state to the $A\,^1\Pi$ state. However, for the other halogen atoms, Br and I, where the spin–orbit constant is large, the excitation process is more complicated since (spin-forbidden) transitions to the $^3\Pi_1$, $^3\Pi_0$, and $^3\Sigma_1^+$ states can occur more readily. As the HX molecule fragments, the initial populations of these states can redistribute among all of the accessible electronic states to yield halogen atoms in both ground, X, and excited, X^*, spin–orbit states.

The relative yield of the two product spin–orbit states is characterized by the excited state, X^*, branching fraction

$$\Gamma = \frac{\sigma(X^*)}{\sigma(X)+\sigma(X^*)}, \tag{2}$$

where $\sigma(X)$ and $\sigma(X^*)$ are the cross-sections for the production of ground and excited state halogen atoms.

The hydrogen halides HCl,[1–13] HBr,[14–21] and HI[22–31] have received extensive experimental and theoretical investigation. However, there has been only one experimental investigation of the spin–orbit branching in HF.[32] The main reason for the lack of study is due to the experimental difficulties in dealing with HF; namely, its highly corrosive nature and an absorption that lies in the vacuum ultraviolet (VUV).[33–35] But while it is experimentally difficult to investigate, HF provides an ideal system to investigate theoretically.

Wittig and co-workers[32] have used the Rydberg time-of-flight technique for hydrogen atoms to obtain the spin–orbit state distribution of the fluorine fragment for HF photodissociation.[32] Using a photoexcitation wavelength of 193.3 nm, the branching fraction of excited state fluorine from the $v=3$ state was determined to be 0.42 ± 0.02 [branching ratio $\sigma(F^*)/\sigma(F)=0.71\pm0.03$]. As a by-product of this work, a branching fraction of 0.41 ± 0.08 (branching ratio$=0.69\pm0.14$) was also determined for the photodissociation from the ground vibrational state ($v=0$) of HF using a photoexcitation wavelength of 121.6 nm. Note that the uncertainty associated with the branching fraction from the $v=0$ level is much greater than that associated with that from the $v=3$ level. These two branching fractions represent all of the available experimental data for HF and no studies as a

[a]Current address: Department of Physics and Astronomy, University of Alabama, Box 870324, Tuscaloosa, Alabama 35487-0324.
[b]Author to whom correspondence should be addressed. Electronic mail: Gabriel.Balint-Kurti@bristol.ac.uk

function of photolysis wavelength have been carried out as has been done for HCl,[1,2] HBr,[15] and HI.[22,23]

This article reports the first theoretical study of the spin–orbit branching in the photodissociation of HF. Section II details how the time-dependent wave packet technique was used to determine the total and partial cross-sections, and, subsequently, the F* branching fraction over a large excitation energy region. New *ab initio* calculations of the potential energy curves and the spin–orbit coupling between these states are reported in Sec. III. These potential energy curves and couplings have then been used to study the dissociation dynamics following photoexcitation from the ground vibrational ($v=0$) state for both HF and DF. The results are reported in Sec. IV and a comparison is made between the two species. The HF branching fraction is compared with the only available experimental result[32] and predictions are made for the branching fraction as a function of photolysis wavelength. Vibrationally mediated photodissociation of HF and DF, for the initial states $v=1$, 2, and 3, is discussed in the following article of this volume. A comparison between HF/DF photodissociation and the photodissociation of HCl/DCl is drawn, and possible reasons for differences between the fluorine and chlorine species are discussed. Finally, some brief conclusions are drawn in Sec. V.

II. PHOTODISSOCIATION DYNAMICS: THEORY

The time-dependent treatment of the photodissociation dynamics is based on the solution of the time-dependent Schrödinger equation

$$i\frac{\partial\Psi(R,t)}{\partial t}=\hat{H}(R)\Psi(R,t), \tag{3}$$

where the time-independent Hamiltonian, $\hat{H}(R)$, is the sum of the nuclear kinetic energy operator, $\hat{T}$, the electronic potential energy, $V(R)$, and the spin–orbit Hamiltonian, H_{so},

$$\hat{H}(R)=\hat{T}+V(R)+H_{\mathrm{so}}(R)=\hat{T}+V_{\mathrm{tot}}(R). \tag{4}$$

Previous time-independent calculations for the photodissociation of HCl[2,7] and HBr[5,14] have included the effects of rotation. However, the effect of rotation on the branching fraction has been shown to be negligible, and, for the time-dependent calculations considered in this article, we feel justified neglecting the rotational coupling.

Within the time-dependent framework,[36,37] the photodissociation dynamics on multiple potential energy curves are followed after setting up initial wave functions (wave packets) given by the product of the transition dipole moment functions with the bound state initial wave function. Expressing this in matrix form, the initial wave packets are given by

$$\Phi(R,t=0)=\mu(R)\Psi(R), \tag{5}$$

where $\Phi(R,t=0)$ represents an n-state column vector, $[\phi_1(R,t=0),\phi_2(R,t=0),\ldots,\phi_n(R,t=0)]^T$ of the wave packets associated with each of the excited state surfaces, $\Psi(R)$ is the ground state wave function, and $\mu(R)$ is a column vector representing the transition moments between the ground state and the excited states. In the form that the equations are presented here, $\mu(R)$ is a single component of a vector function. Spherical vectors[38] are used because these are consistent with the use of the Ω quantum number.

The resulting wave functions are then propagated on the excited state surfaces in a series of short time steps.[37] After each time step, a contribution to the autocorrelation function,

$$A(t)=\int_{R_{\min}}^{R_{\max}}\Phi^*(R,t=0)\Phi(R,t)dR$$
$$=\sum_{i=1}^{n}\int_{R_{\min}}^{R_{\max}}\phi_i^*(R,t=0)\phi_i(R,t)dR, \tag{6}$$

is calculated and accumulated.

The total cross-section as a function of the frequency of the incident radiation is given by the Fourier transform of the autocorrelation function as a function of time.[36,37] The total integral cross-section in SI units is

$$\sigma^{\mathrm{tot}}(\nu)=\frac{2\pi\nu}{3c\varepsilon_0\hbar}\int_0^{\infty}\exp[i(E_i+h\nu)t/\hbar)]A(t)dt. \tag{7}$$

However, in order to determine the branching fraction, it is necessary to determine the partial absorption cross-sections. The partial absorption cross-sections can be calculated by examining the wave packet on each excited state surface at a large internuclear separation (R_∞) such that the wave packet is in the asymptotic region where there is no longer coupling between the excited states. It can be shown[37,39] that the partial cross-section for channel n as a function of photon energy, $\sigma_n(\nu)$, is given by

$$\sigma_n(\nu)=\frac{4\pi^3\nu k_n}{3c\varepsilon_0 m}|A_n(R_\infty,E)|^2, \tag{8}$$

where

$$A_n(R_\infty,E)=\frac{1}{2\pi}\int_0^{\infty}\phi_n(R_\infty,t)\exp[i(E_i+h\nu)t/\hbar]dt, \tag{9}$$

m is the reduced mass of the two photofragments, and k_n is the magnitude of the wave vector of the relative motion.

The calculations are performed using uniformly spaced grids for both the internuclear coordinate and the momentum conjugate to it.[37] As the wave packets reach the asymptotic region of the coordinate grid, they must be damped out, otherwise the periodic nature of the Fourier transforms would cause them to reappear at the small R end of the grid. Therefore, the asymptotic wave functions were damped using a complex absorbing potential.[37,40] We have used a cubic complex absorbing potential defined by

$$V_{\mathrm{damp}}(R)=\begin{cases}0.0, & R<R_{\mathrm{damp}}\\ -iA_{\mathrm{damp}}\left(\dfrac{R-R_{\mathrm{damp}}}{R_{\max}-R_{\mathrm{damp}}}\right)^3, & R_{\mathrm{damp}}\leqslant R\leqslant R_{\max}\end{cases}, \tag{10}$$

where R_{damp} is the point where the damping is switched on, and A_{damp} is an optimized parameter giving the strength of the damping.

The photodissociation of HF can be treated as a three (excited) state problem, where the states which must be considered are $^1\Pi_{\Omega=1}$, $^3\Pi_{\Omega=1}$, and $^3\Sigma_{\Omega=1}$. We have neglected

the direct excitation to the $^3\Pi_{\Omega=0^+}$ state since the *ab initio* calculations (see next section) revealed that its contribution was negligibly small.

Two different electronic bases are used: (i) a diabatic basis, in which Λ, S^2, and Σ are good quantum numbers and the spin–orbit interaction has off-diagonal matrix elements coupling the states, and (ii) a fully adiabatic basis in which the spin–orbit interaction is diagonal and the coupling between the states is due to off-diagonal terms in the kinetic energy. The initial column wave function, see Eq. (5), in the diabatic basis is given by

$$\begin{pmatrix} \phi_1(R,t=0) \\ \phi_2(R,t=0) \\ \phi_3(R,t=0) \end{pmatrix} = \begin{pmatrix} 0 \\ \mu_2(R)\chi(R) \\ 0 \end{pmatrix}, \tag{11}$$

where $\mu_2(R)$ is the $A\,^1\Pi \leftarrow X\,^1\Sigma^+$ transition moment and $\chi(R)$ is the ground vibrational state wave function as determined using the Fourier grid Hamiltonian method.[37,41] In the diabatic basis, there are no direct transitions to the $^3\Pi_1$ and $^3\Sigma_1$ states as both of these transitions are spin-forbidden.

The relationship between the fully adiabatic basis and the diabatic basis can be expressed as

$$\phi^{\mathrm{ad}}(R) = \mathbf{M}(r)\,\phi^{\mathrm{diab}}(R), \tag{12}$$

where $\mathbf{M}(R)$ is the matrix which continuously diagonalizes the total potential energy matrix, in our case, $V_{\mathrm{tot}}(R) = V(R) + H_{\mathrm{so}}(R)$, at each value of the internuclear separation. In other words, the fully adiabatic wave function for a particular state can be written as a superposition over the diabatic states which can contribute to it, i.e.,

$$\phi_j^{\mathrm{ad}}(R) = \sum_i m_{ji}(R)\,\phi_i^{\mathrm{diab}}(R), \tag{13}$$

where the $m_{ji}(R)$ are the elements of the diabatic-to-adiabatic transformation matrix $\mathbf{M}(R)$.

From the fully adiabatic wave functions, we can define the fully diagonal adiabatic potential energy curves,

$$V^{\mathrm{ad}}(R) = \mathbf{M}(R)\,V_{\mathrm{tot}}(R)\,\mathbf{M}^T(R). \tag{14}$$

Expressing the matrix explicitly for the 3×3 problem under consideration, we have

$$\begin{pmatrix} V_1^{\mathrm{ad}} & 0 & 0 \\ 0 & V_2^{\mathrm{ad}} & 0 \\ 0 & 0 & V_3^{\mathrm{ad}} \end{pmatrix} = \mathbf{M}(R) \begin{pmatrix} V_1^{\mathrm{diab}} & H_{\mathrm{so}}^{12} & H_{\mathrm{so}}^{13} \\ H_{\mathrm{so}}^{21} & V_2^{\mathrm{diab}} & H_{\mathrm{so}}^{23} \\ H_{\mathrm{so}}^{31} & H_{\mathrm{so}}^{32} & V_3^{\mathrm{diab}} \end{pmatrix} \mathbf{M}^T(R), \tag{15}$$

where $1 \equiv {}^3\Pi_{\Omega=1}$, $2 \equiv {}^1\Pi_{\Omega=1}$, and $3 \equiv {}^3\Sigma_{\Omega=1}$, and we have dropped the explicit dependence upon the internuclear distance R. It should be noted that the labels $^1\Pi$, $^3\Pi$, $^3\Sigma$ used in the adiabatic representation only refer to the major contributing diabatic state in the Franck-Condon region, i.e., the diabatic state with the largest coefficient m_{ji}, see Eq. (13), for $R<3$ bohr. The only good quantum number in the fully adiabatic representation is Ω.

The photodissociation dynamics are performed using the fully adiabatic representation as the primary representation. The Chebychev propagation scheme[42] was used to solve the time-dependent Schrödinger equation. In order to properly account for the nonadiabatic kinetic energy coupling of the three adiabatic $\Omega=1$ surfaces considered here, a modified Chebychev propagation scheme must be used. When acting with the kinetic energy part of the Hamiltonian, the modified Chebychev method requires (i) two transformations, $\mathbf{M}(R)$ and $\mathbf{M}^T(R)$, to change between the diabatic basis and the fully adiabatic basis, see Eq. (12), and (ii) two fast Fourier transforms to switch between the coordinate representation and the momentum representation. The fast Fourier transformations are needed to act with the kinetic energy operator, which is diagonal in the momentum representation but not in the coordinate representation. Note that the Fourier transformation is performed in the diabatic basis in which the kinetic energy operator is diagonal. The other transformations are needed to act with the total potential energy, $V^{\mathrm{ad}}(R)$, which is diagonal in the fully adiabatic basis but is not diagonal in the diabatic basis. The physically meaningful results are those obtained in the fully adiabatic basis. Therefore, the wave packets which are analyzed using Eq. (9) are the $\phi_n^{\mathrm{ad}}(t)$'s.

III. *AB INITIO* CALCULATIONS

There have been many previous theoretical studies of both the ground state, see, for example, the benchmark calculations of Dunning and co-workers,[43] and also of the excited states[44–47] of HF. In this study, we are only interested in those states, $^1\Sigma^+$, $^1\Pi$, $^3\Pi$, $^3\Sigma^+$, which correlate with the lowest energy asymptote, $\mathrm{H}(^2S)+\mathrm{F}(^2P)$.

The calculations of the diabatic potential energy curves have been carried out using the augmented correlation-consistent valence quintuple zeta ($av5z$) basis set of Dunning *et al.*[48] For the hydrogen atom, the $(9s5p3d2f1g)/[5s4p3d2f1g]$ contraction was used and for the fluorine atom, the $(15s9p5d34f3g2h)/[6s5p4d3f2g1h]$ contraction was employed. Using this $av5z$ basis resulted in a total of 146 contracted functions.

In order to determine the potential energy curves, complete active space self-consistent field (CASSCF) calculations[49,50] were first performed. The active space comprised eight electrons in five orbitals (the $1s$ orbital on the fluorine atom was excluded). The CASSCF optimization was performed for each state separately in order to obtain the ''best'' representation. These CASSCF orbitals and wave functions were then used as a starting point for multireference internally contracted configuration interaction (MRCI)[51,52] calculations, again excluding the $1s$ orbital of fluorine. The effect of higher-order excitation was estimated using the Davidson correction.[53] The reference spaces consisted of 8, 3, 3, and 3 configuration state functions for the $^1\Sigma^+$, $^1\Pi$, $^3\Pi$, and $^3\Sigma^+$ states, respectively. While a larger number of reference configurations has been used in studies including the low-lying Rydberg states,[44,45] the small number of CSFs used here provides an adequate description of the low-lying valence states at the CASSCF level, especially in the important asymptotic region. The total number of contracted configurations was 116 462, 116 653, 117 158, and 116 615 for the $^1\Sigma^+$, $^1\Pi$, $^3\Pi$, and $^3\Sigma^+$ states, respectively. All calculations reported in this article were performed using

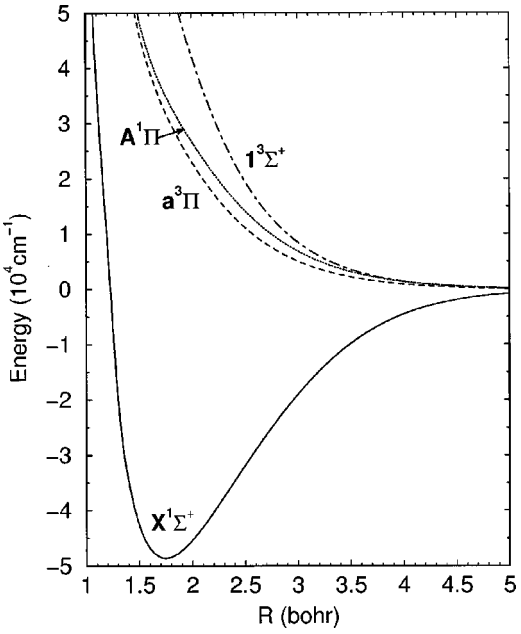

FIG. 1. Potential energy curves for the $X\,^1\Sigma^+$, $^1\Pi$, $^3\Pi$, and $^3\Sigma$ diabatic states of HF as determined by *ab initio* MRCI calculations.

the MOLPRO *ab initio* molecular electronic structure program.[54]

As with HCl,[2,7] the fine-structure splitting in HF will be strongly influenced by the shape of the potential energy curves in the asymptotic region, where the energy separations of the diabatic states are of comparable magnitude to the spin–orbit splitting in the F atom ($404.1\,\mathrm{cm}^{-1}$). Therefore, it is of utmost importance to obtain an accurate representation of the energies in this region. In order to achieve this goal, we include the standard counterpoise correction for basis set superposition error[55] to the calculated interaction energy. This counterpoise correction can be written as

$$\Delta E_{\mathrm{cp}}(R)=\Delta E_{\mathrm{H}}(R)+\Delta E_{\mathrm{F}}(R), \tag{16}$$

where $E_i(R)$ is the energy of atom i determined in the full orbital space of the supermolecule at the same internuclear distance R minus the energy computed using the basis functions associated only with that atom. Also, we include a correction for the remaining size consistency error of the MRCI calculations

$$\Delta E_{\mathrm{sc}}=E_{\mathrm{HF}}(\infty)-E_{\mathrm{H}}(\infty)-E_{\mathrm{F}}(\infty). \tag{17}$$

This correction was determined to be $+13.8\,\mathrm{cm}^{-1}$ for the Σ states and $-12.1\,\mathrm{cm}^{-1}$ for the Π states. For the H atom, these energies were computed at the restricted Hartree–Fock level of theory. From these calculations, the total interaction energy can be expressed as

$$V(R)=E_{\mathrm{MRCI}}(R)-E_{\mathrm{H}}(\infty)-E_{\mathrm{F}}(\infty)-\Delta E_{\mathrm{cp}}(R)-\Delta E_{\mathrm{sc}}. \tag{18}$$

Figure 1 illustrates the resulting potential energy curves for the lowest four states of HF. These potential energy curves will be referred to as the diabatic states. In this representation, the only optically allowed transition is from the ground state to the $A\,^1\Pi$ state. From the potential energy curves, the vertical excitation energy to the $A\,^1\Pi$ state at $R=1.7375$ bohr, is $84\,205\,\mathrm{cm}^{-1}$. This result agrees to within 3% with several other calculated vertical excitation energies from the ground state to the $A\,^1\Pi$ state, see Table I. The comparison includes results[44,45] which have used a much larger number of reference configurations for the MCSCF part of the calculation. We can conclude that the more limited number of reference configurations used in the present calculation has provided a good representation of the $X\,^1\Sigma^+$ and $A\,^1\Pi$ states.

TABLE I. Vertical excitation energies to the $A\,^1\Pi$ state.

Calculation	Energy (cm^{-1})	% Difference[a]
Present calculation	84 205	
Ref. 44[b,c]	85 172	−1.1
Ref. 44[b,d]	83 962	+0.3
Ref. 45[b]	87 083	−3.4
Ref. 46[b]	86 301	−2.5

[a]Determined as $(84\,205-E)*200/(84\,205+E)$.
[b]Results for $R=1.7329$ bohr.
[c]MR-CI result.
[d]Full CI estimation.

The computed $X\,^1\Sigma^+$ ground state has been used to determine the energies of the lowest four vibrational states of HF by utilizing the Fourier grid Hamiltonian method.[37,41] The computed energies are compared with results which have been determined previously from fitting experimental data,[56,57] see Table II. From the excellent agreement obtained with these results, we believe that we have an accurate representation of the ground state potential energy curve.

The $A\,^1\Pi \leftarrow X\,^1\Sigma^+$ electronic transition moment was obtained using a slightly different procedure than that used for the computation of the potential energy curves while utilizing the same $av5z$ basis set. In order to compute a transition moment, it is necessary to have a common set of orbitals and a well-defined wave function to describe both states involved. Therefore, the state-averaged CASSCF (SA-CASSCF) method[49,50] was used to obtain a single set of CASSCF orbitals for the singlet Σ and Π states. From this starting point, MRCI calculations were performed to obtain the transition moment.

The $A\,^1\Pi \leftarrow X\,^1\Sigma^+$ transition moment as a function of HF bond distance is illustrated in Fig. 2. As expected, the transition moment in HF demonstrates qualitatively similar behavior to the transition moment in HCl.[7,13] The increase in the transition moment as the internuclear distance decreases

TABLE II. Vibrational energy levels for the $X\,^1\Sigma^+$ ground state of HF. Values are measured from the minimum on the ground state potential energy curve and are given in cm^{-1}.

Vibrational state	Present calculation[a]	Ref. 56[b]	Ref. 57[c]
0	2057.4	2046.69	2046.82
1	6034.1	6005.25	6008.25
2	9841.1	9784.05	9797.66
3	13 483.7	13 383.08	13 419.85

[a]Obtained using the Fourier grid Hamiltonian method (Refs. 37, 41).
[b]Obtained by fitting experimental data.
[c]Obtained by simultaneously fitting the HF and DF experimental data.

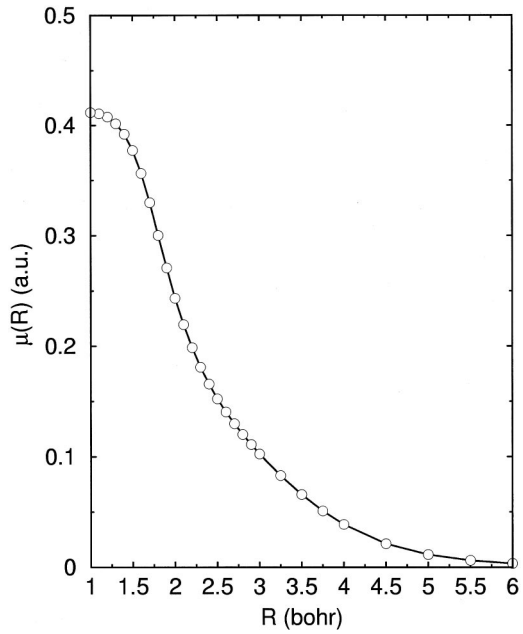

FIG. 2. The $A\,^1\Pi \leftarrow X\,^1\Sigma^+$ electronic transition moment as a function of the HF bond distance, as determined by the MRCI calculations. The transition moment is given in atomic units.

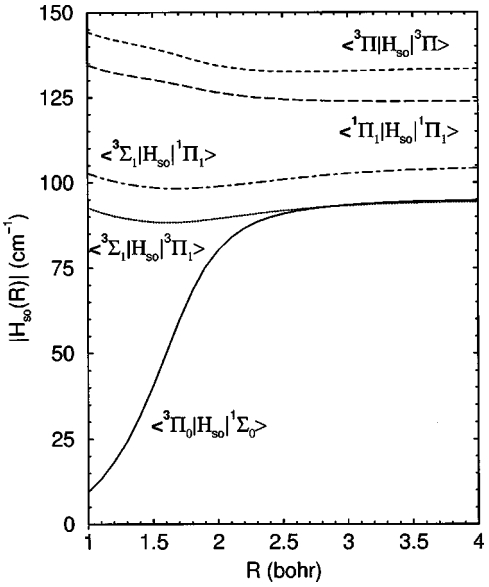

FIG. 3. The spin–orbit coupling matrix elements as a function of the HF bond distance as determined by the CASSCF calculations. For clarity, the couplings between the $^3\Sigma_1^+$ and $^1\Pi_1$ diabatic states and between the $^1\Pi_1$ and $^1\Pi_1$ diabatic states have been shifted by plus and minus $10\,\mathrm{cm}^{-1}$, respectively.

is a feature of all of the hydrogen halides and arises from the increase in the ionic character of the ground $X\,^1\Sigma^+$ state at smaller bond lengths.

Finally, the spin–orbit matrix elements were determined using a procedure which differed from both the calculation of the potential energy curves and the electronic transition moment. In order to describe singlet–singlet, singlet–triplet, and triplet–triplet coupling, it is necessary to have a common set of orbitals for all states. Therefore, the SA-CASSCF method was used to calculate a common set of orbitals for the $^1\Sigma^+$, $^1\Pi$, $^3\Pi$, and $^3\Sigma^+$ states. These orbitals and wave functions were then used to compute the spin–orbit matrix elements at the CASSCF level. At this level of theory, the fluorine atom fine-structure splitting, $E(^2P_{1/2})-E(^2P_{3/2})$, was calculated to be $401.4\,\mathrm{cm}^{-1}$ which is within 1% of the experimental value[58] of $404.1\,\mathrm{cm}^{-1}$. For the spin–orbit calculations, the basis set had to be restricted to $(9s5p4d3f)/[5s4p3d2f]$ for the H atom and $(15s9p5d4f)/[6s5p4d3f]$ for the fluorine atom.

The spin–orbit coupling between the various singlet and triplet diabatic states as a function of the HF internuclear distance is illustrated in Fig. 3. The couplings between the $^3\Sigma_1^+$ and $^1\Pi_1$ states and between the $^1\Pi_1$ and $^1\Pi_1$ states have been shifted by plus and minus $10\,\mathrm{cm}^{-1}$, respectively, for clarity. The couplings for HF as calculated using the CASSCF wave functions have a nearly identical form to the calculations for HCl, see Fig. 2 in Ref. 7, which employed a simplified treatment of the orbital angular momentum.

From the diabatic potential energy curves and the spin–orbit couplings, the fully adiabatic potentials are determined by diagonalizing V_{tot} of Eq. (4). The fully adiabatic potentials and the matrix, $\mathbf{M}(R)$, which transforms from the diabatic to the adiabatic representation, are both needed in order to perform the time-dependent wave packet dynamics. The fully adiabatic energies are illustrated in Fig. 4. The states are labeled by the case (a) diabatic state making the largest contribution to the fully adiabatic state in the Franck–Condon region and by the quantum number Ω. The figure shows the adiabatic potentials for $\Omega=0$, $\Omega=1$, and $\Omega=2$. The figure is in two parts, corresponding to *e* and *f* parity states[59] for the case $J=0$. Only the $\Omega=1$ curves are used in the dynamical calculations reported below.

IV. PHOTODISSOCIATION DYNAMICS: RESULTS AND DISCUSSION

The initial photoexcitation of the HF molecule is treated as a two-state problem involving the ground $X\,^1\Sigma^+$ and excited $A\,^1\Pi$ *diabatic* states. However, as the molecule fragments, the initial excitation is redistributed on to the other accessible states. When the molecule is fully dissociated, the fragments end up on one of the two accessible *adiabatic* asymptotes. How this redistribution occurs depends intimately upon the dynamics of the process. However, by examining the diabatic-to-adiabatic transformation matrix, $\mathbf{M}(R)$, details of the redistribution can be elucidated. In Fig. 5, the diabatic-to-adiabatic transformation matrix has been illustrated by plotting the modulus of m_{ji} for each resulting adiabatic state. From Fig. 5, it is clear that there is no appreciable mixing of the singlet and triplet states for $R<3$ bohr, so the assumption that the initial excitation can be treated as a two state problem is valid. The mixing of the states changes drastically over the region $3\leqslant R\leqslant 9$ bohr. It is within this region that the important dynamics will take place.

Using the calculated adiabatic *ab initio* potentials and the diabatic-to-adiabatic transformation matrices, the method outlined in Sec. II has been used to obtain the photodissociation cross-sections. The solid line in Fig. 6 illustrates the

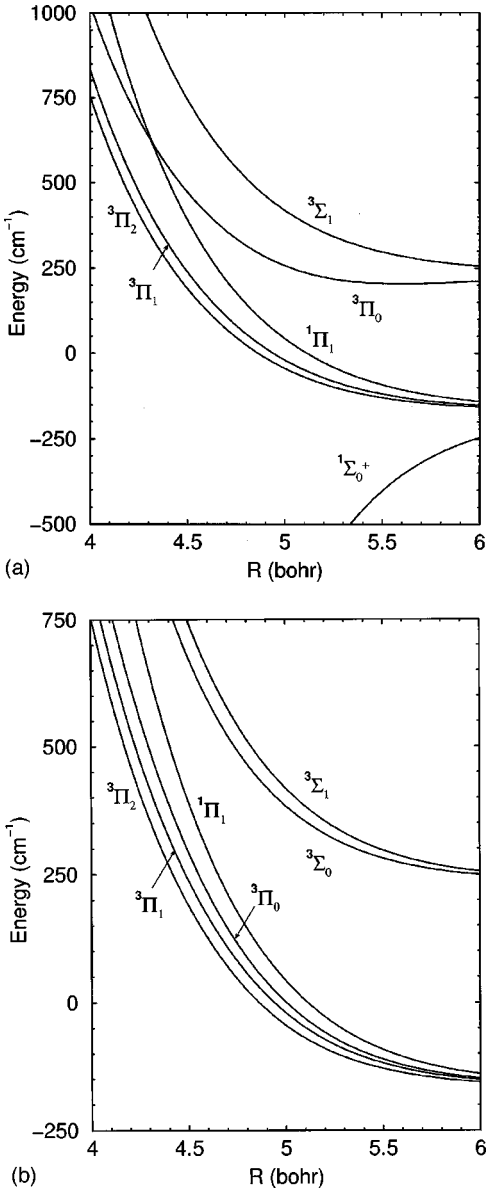

FIG. 4. The fully adiabatic potential energy as a function of the HF bond distance. Figure 4(a) shows the even parity or *e* state potential energy curves for $J=0$, while Fig. 4(b) shows the odd parity or *f* curves.

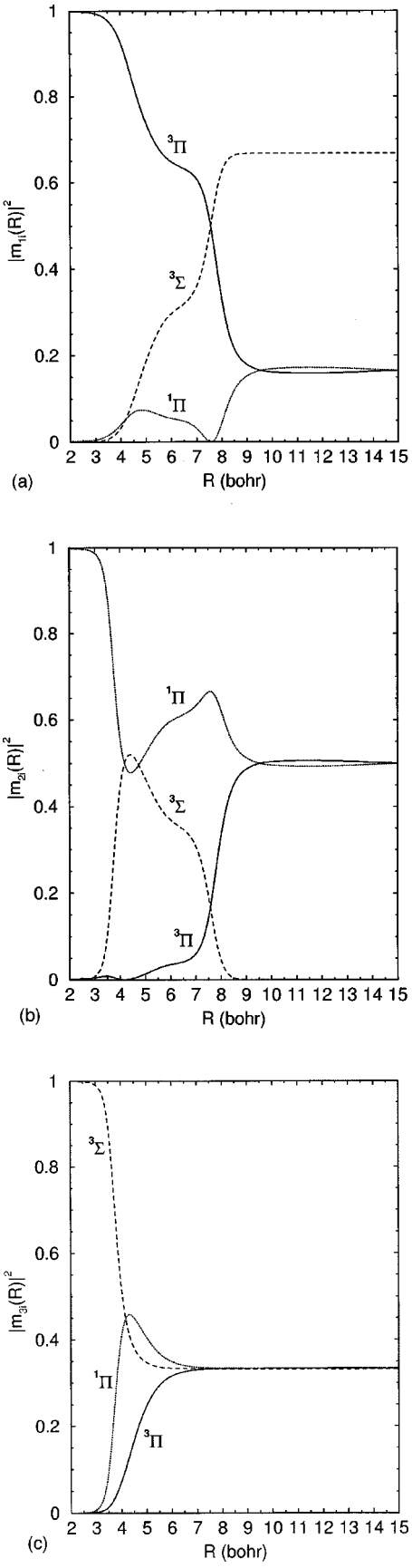

FIG. 5. The contribution $|m_{ji}|^2$ of the diabatic states to the fully adiabatic states, $\phi_j^{\mathrm{ad}}(R)=\Sigma_i m_{ji}(R)\phi_i^{\mathrm{diab}}(R)$, as a function of internuclear separation for the adiabatic states (a) $^3\Pi_1$, (b) $^1\Pi_1$, and (c) $^3\Sigma_1$. The fully adiabatic states are labeled with the diabatic state which contributes the most within the Franck–Condon region and with the good quantum number Ω.

calculated total photodissociation cross-section for HF. To the best of the authors' knowledge, this represents the first-calculation of the HF absorption spectrum, although there have been previous determinations of the oscillator strength of this transition.[33,44,47] Also displayed are the experimental values of Hitchcock *et al.*[33] and Nee *et al.*[34] The experimental results of Nee are a factor of two smaller than the results of Hitchcock but no explanation for this experimental discrepancy has been given.[34] Our total cross-sections calculated at 121.6 nm (82 237 cm^{-1}) and 145 nm (68 966 cm^{-1}) are $3.1\times10^{-18}\,\mathrm{cm}^2$ and $0.5\times10^{-18}\,\mathrm{cm}^2$, respectively, as compared to the values reported in Ref. 34 of $3.3\times10^{-18}\,\mathrm{cm}^2$ and $1.7\times10^{-18}\,\mathrm{cm}^2$. The calculated total cross-section supports the experimental results of Nee and coworkers but it would be beneficial to resolve the experimental discrepancies.

Included in Fig. 6 is the total photodissociation cross-

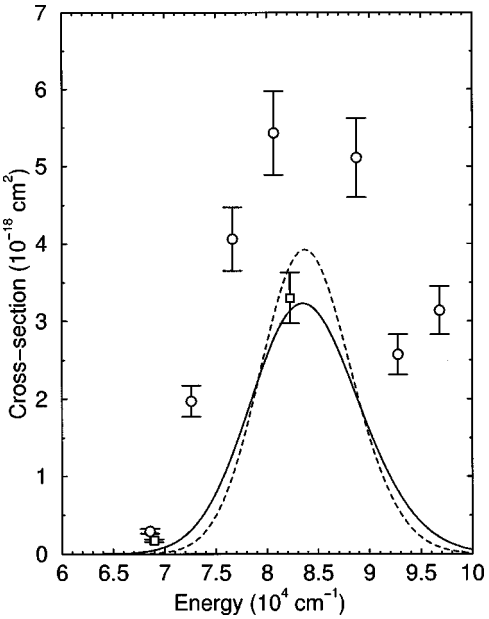

FIG. 6. The total photodissociation cross-section for $A\,^1\Pi \leftarrow X\,^1\Sigma^+$ dissociation out of the $v=0$ vibrational level for HF (solid line) and DF (dashed line) as a function of photon energy. Also, shown are the experimental values of Hitchcock *et al.* (Ref. 33) (circles) and Nee *et al.* (Ref. 34) (squares). The experimental results have been illustrated with error bars of $\pm 10\%$.

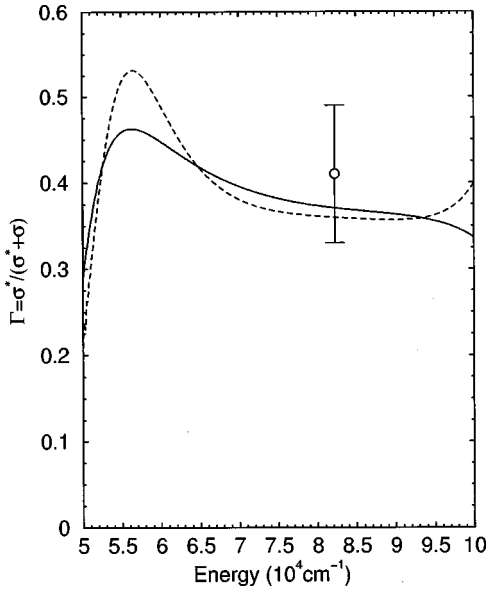

FIG. 7. The F atom excited state branching fraction, $\Gamma=\sigma(F^*)/[\sigma(F^*)+\sigma(F)]$, as a function of photon energy for the photodissociation of HF (solid line) and DF (dashed line) out of the $v=0$ vibrational state. Also, shown is the experimental value for HF of Wittig and co-workers (Ref. 32) for the wavelength 121.6 nm (82 237 cm^{-1}).

section for the deuterated fluorine species, DF (dashed line). The total absorption cross-section for DF has not been measured experimentally, but the relationship between the calculated HF and DF cross-sections is very similar to that between those measured for HI and DI.[31] In both cases, the deuterated species has a total cross-section which peaks at a higher energy (due to the change in the initial vibrational energy), a larger peak magnitude, and a slightly narrower profile.

The calculated branching fractions, see Eq. (2), for both HF and DF as a function of the excitation energy are illustrated in Fig. 7 for excitation from the ground vibrational state ($v=0$). For a wavelength of 121.6 nm (82 237 cm^{-1}), the calculated value of 0.37 compares quite well with the experimentally measured value of 0.41 ± 0.08.[32] Both the HF and the DF results show a maximum value in the production of F* for low excitation energies. The branching fraction maximum for HF is 0.46 and occurs at approximately 57 000 cm^{-1}. For DF, the peak value is 0.53 and occurs at approximately 56 500 cm^{-1}. The HF and DF branching fractions are then quite similar across the rest of the illustrated excitation energy range except at very high energy ($>90\,000$ cm^{-1}) where the branching fraction for HF begins to decrease while that for DF increases. These high energy results should be interpreted with a great deal of caution as previous experiments[33] and calculations[44,45] have shown that other excited electronic states are accessible at these energies.

Several simplified models have been discussed for estimating the excited state branching fraction. These may be categorized as the ''sudden'' model, the ''strong coupling'' model, and the ''adiabatic'' model. In the sudden model, the atoms are pictured as separating very rapidly, and it is assumed that there is insufficient time for the electronic structure to change slowly so as to follow the adiabatic correlation diagram (Fig. 4). This model has also been called the ''diabatic'' model.[18] The hydrogen halides form the best candidates for complying with this model as the speed of the H atom recoil is enhanced by its light mass relative to the mass of its halogen atom partner. Figure 8(a) shows the component of the $^1\Pi$ diabatic state, as a function of the internuclear separation, for each of the three fully adiabatic $\Omega=1$ states which are involved in the dynamics. This figure is useful in discussing the three models mentioned above. The three curves are identified with the labels F or F* to indicate the asymptotic energies of the corresponding adiabatic states. The asymptotic values of the lines in Fig. 8(a) give the sudden model limit for the population of the excited and ground spin–orbit states. The sudden limit, which has been discussed by Matsumi *et al.*[18] and by Singer and Freed,[60] results in one third of the population in the F* excited state and two thirds in the ground spin–orbit state. In the strong coupling limit, also referred to as the ''statistical'' limit, it is assumed that the states are so strongly coupled by the interaction that all accessible states are equally populated. It also results in one-third of the population in the excited spin–orbit state and two-thirds in the ground state. In contrast, the adiabatic model assumes that the fragments part slowly and that, as the molecule passes through each avoided curve crossing, it remains in a single adiabatic state. In the present case, as the initial excitation is to the $^1\Pi_1$ adiabatic state [equal to the $^1\Pi$ diabatic state in the Franck–Condon region, see Fig. 5(b)], all of the population would end up in the lower spin–orbit

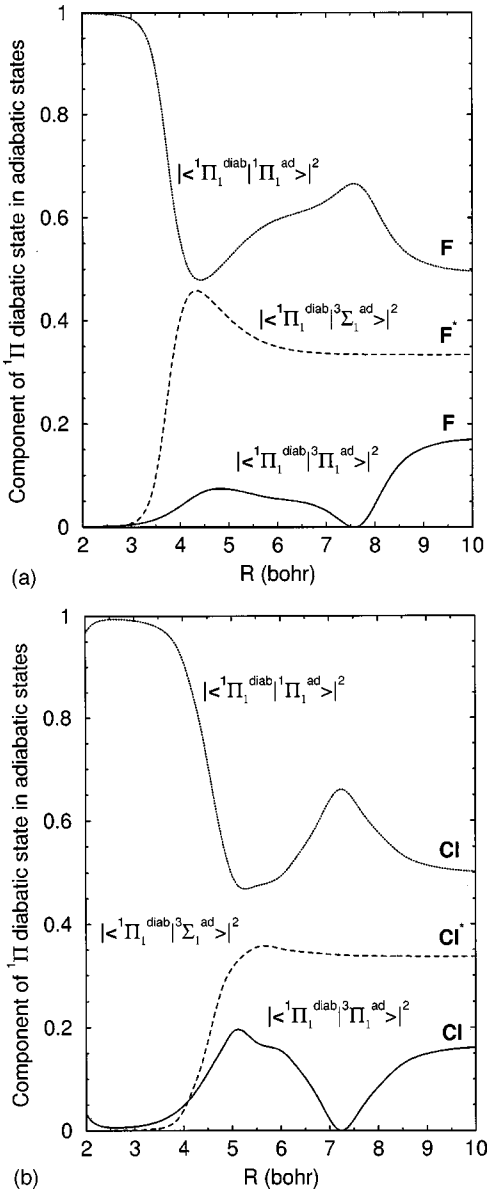

FIG. 8. A plot of the contribution of the $^1\Pi$ diabatic state to the fully adiabatic states as a function of the bond distance, see Eq. (13), for (a) HF and (b) HCl. The HCl results are based on the potential energy curves and off-diagonal couplings calculated in Ref. 7.

level (see Fig. 4), corresponding to an excited state branching fraction of zero.

The actual computed excited state branching fraction (Fig. 7) varies with energy and does not conform to the statistical limit, which would be predicted by both the sudden and the strong coupling models, or to the adiabatic limit. The energy dependence of this ratio is a sensitive diagnostic for the details of the dynamics of the system and constitutes a stringent test of the correctness of the potentials and the coupling matrix elements used as well as of the methodology employed. It is interesting to note from Fig. 8(a) that the contribution of the $^1\Pi_1$ diabatic state to the $^3\Sigma_1$ adiabatic state peaks at $R=4.325$ bohr, having a value of 0.46 at this point.

When comparing the branching fractions for HF vs. DF to the corresponding results for HCl and DCl,[2,7] a remarkable difference is seen. While the branching fractions for HF and DF are very similar over the entire excitation energy range, the branching fraction for DCl is much lower than that for HCl. The branching fraction for HCl shows a maximum as a function of energy similar to that displayed by HF and DF, but the branching fraction for DCl has no such maximum.[2] Alexander and co-workers[2,7] explain the differences between the HCl and DCl branching fractions by ''the reduced tendency for the system with heavier reduced mass to undergo nonadiabatic transitions, especially at lower values of the excitation frequency, where the relative velocity of the nascent fragments will be smaller.'' Based upon this simple qualitative argument, similar results would have been expected in DF relative to HF. Contrary to this, the calculations show that the DF results are very similar to those for HF and, in particular, exhibit an excited state branching fraction larger than the one for HF at low excitation energies. Figure 8(b) shows the component of the $^1\Pi$ diabatic state in each of the three fully adiabatic $\Omega=1$ states for HCl as determined using the diabatic potential energy curves and corresponding off-diagonal spin–orbit couplings of Alexander and co-workers.[7] If this figure is compared with Fig. 8(a), we see that the maximum in the $|\langle {}^1\Pi_1^{\rm diab}|{}^3\Sigma_1^{\rm adiab}\rangle|^2$ coefficient curve is absent for HCl. It seems clear that this mixing coefficient, and its variation with internuclear separation, plays an important role in the nonadiabatic dynamics of the photodissociation process.

V. CONCLUSIONS

Accurate potential energy curves and transition dipole moment functions have been calculated for the low-lying states of HF. These have been used to compute both absolute absorption cross-sections and excited spin–orbit state branching fractions for both HF and DF from their ground vibrational states. The excited spin-orbit state branching fraction is found to be nonstatistical. Both the statistical and the sudden limit models predict a branching fraction of 1/3. The calculated branching fractions are higher than this and vary with photon energy. This shows clearly that nonadiabatic dynamical effects play an important role in the photodissociation dynamics. For both HF and DF, the calculations predict a peak in the branching fraction at low photon energy. A similar peak has been predicted and observed experimentally for HCl[2,7] but is determined, both theoretically[7] and experimentally,[8–10] not to be present for DCl. In contrast, DF is predicted to have a larger peak in the branching fraction vs photon energy curve than HF. While it will be experimentally difficult, there is clearly a need to determine the branching fraction for HF following excitation from the ground vibrational state more precisely and for a wider range of excitation energies than are presently available. We also hope that the theoretical results presented here will stimulate an experimental confirmation, or refutation, of the interesting behavior, as a function of photon energy, in the branching fraction for DF, relative to its DCl counterpart.

ACKNOWLEDGMENTS

A.B. would like to thank the Natural Sciences and Engineering Research Council of Canada for the award of a postdoctoral fellowship. We would like to thank Dr. A. J. Orr-Ewing, Professor R. N. Dixon, and Dr. P. M. Regan for many valuable contributions to this work through their contributions to the basic theory and useful discussions about the photodissociation of hydrogen halides. We thank the EPSRC for the provision of funds for the purchase of computational equipment.

[1] P. M. Regan, S. R. Langford, D. Ascenzi, P. A. Cook, A. J. Orr-Ewing, and M. N. R. Ashfold, Phys. Chem. Chem. Phys. **1**, 3247 (1999).
[2] H. M. Lambert, P. J. Dagdigian, and M. H. Alexander, J. Chem. Phys. **108**, 4460 (1998).
[3] J. Zhang, M. Dulligan, and C. Wittig, J. Chem. Phys. **107**, 1403 (1997).
[4] R. Liyanage, Y. Yang, S. Hashimoto, R. J. Gordon, and R. W. Field, J. Chem. Phys. **103**, 6811 (1995).
[5] T. Duhoo and B. Pouilly, J. Chem. Phys. **103**, 182 (1995).
[6] I. H. Gersonde, S. Henning, and H. Gabriel, J. Chem. Phys. **101**, 1231 (1994).
[7] M. H. Alexander, B. Pouilly, and T. Duhoo, J. Chem. Phys. **99**, 1752 (1993).
[8] K. Tonokura, Y. Matsumi, M. Kawasaki, S. Tasaki, and R. Bersohn, J. Chem. Phys. **97**, 8210 (1992).
[9] Y. Matsumi, P. K. Das, M. Kawasaki, K. Tonokura, T. Ibuki, G. Inoue, S. Satyapal, and R. Bersohn, J. Chem. Phys. **97**, 5261 (1992).
[10] D. Ascenzi, P. M. Regan, and A. J. Orr-Ewing, Chem. Phys. Lett. **310**, 477 (1999).
[11] E. Tiemann, H. Kanamori, and E. Hirota, J. Chem. Phys. **88**, 2457 (1988).
[12] S. C. Givertz and G. G. Balint-Kurti, J. Chem. Soc., Faraday Trans. **82**, 1231 (1986). Note that Eq. (8) of the present article corrects an error in Eq. (25) of this reference. This error originated in the omission of a factor of 4π in the normalization of the continuum wave function [Eq. (3)].
[13] E. van Dishoeck, M. van Hemert, and A. Dalgarno, J. Chem. Phys. **77**, 3693 (1982).
[14] B. Pouilly and M. Monnerville, Chem. Phys. **238**, 437 (1998).
[15] P. M. Regan, S. R. Langford, A. J. Orr-Ewing, and M. N. R. Ashfold, J. Chem. Phys. **110**, 281 (1999).
[16] G. Peoux, M. Monnerville, T. Duhoo, and B. Pouilly, J. Chem. Phys. **107**, 70 (1997).
[17] T. Kinugawa and T. Arikawa, J. Chem. Phys. **96**, 4801 (1992).
[18] Y. Matsumi, K. Tonokura, M. Kawasaki, and T. Ibuki, J. Chem. Phys. **93**, 7981 (1990).
[19] Z. Xu, B. Koplitz, and C. Wittig, J. Phys. Chem. **92**, 5518 (1988).
[20] Z. Xu, B. Koplitz, and C. Wittig, J. Chem. Phys. **87**, 1062 (1987).
[21] F. Magnotta, D. J. Nesbitt, and S. R. Leone, Chem. Phys. Lett. **80**, 21 (1981).
[22] D. J. Gendron and J. W. Hepburn, J. Chem. Phys. **109**, 7205 (1999).
[23] S. R. Langford, P. M. Regan, A. J. Orr-Ewing, and M. N. R. Ashfold, Chem. Phys. **231**, 245 (1998).
[24] N. Chakrabarti and N. Sathyamurthy, J. Phys. Chem. A **102**, 7089 (1998).
[25] C. Kalyanaraman and N. Sathyamurthy, Chem. Phys. Lett. **209**, 52 (1993).
[26] I. Levy and M. Shapiro, J. Chem. Phys. **89**, 2900 (1988).
[27] G. N. A. van Veen, K. A. Mohamed, T. Baller, and A. E. de Vries, Chem. Phys. **80**, 113 (1983).
[28] P. Brewer, P. Das, G. Ondrey, and R. Bersohn, J. Chem. Phys. **79**, 720 (1983).
[29] R. D. Clear, S. J. Riley, and K. R. Wilson, J. Chem. Phys. **63**, 1340 (1975).
[30] R. Schmiedl, H. Dugan, W. Meier, and K. H. Welge, Z. Phys. A **304**, 137 (1982).
[31] J. F. Ogilvie, Trans. Faraday Soc. **67**, 2205 (1971).
[32] J. Zhang, C. W. Riehn, M. Dulligan, and C. Wittig, J. Chem. Phys. **104**, 7027 (1996).
[33] A. P. Hitchcock, G. R. J. Williams, C. E. Brion, and P. W. Langhoff, Chem. Phys. **88**, 65 (1984).
[34] J. B. Nee, M. Suto, and L. C. Lee, J. Phys. B **18**, L293 (1985).
[35] E. Safary, J. Romand, and B. Vodar, J. Chem. Phys. **19**, 379 (1951).
[36] E. J. Heller, J. Chem. Phys. **68**, 2066 (1978); **68**, 3891 (1978); Acc. Chem. Res. **14**, 368 (1981).
[37] G. G. Balint-Kurti, R. N. Dixon, and C. C. Marston, Int. Rev. Phys. Chem. **11**, 317 (1992); the first line of Eq. (52) of this article should read
$$H_{ij}^0=\frac{h^2}{4mL^2}\left[\frac{(N-1)(N-2)}{6}+\frac{N}{2}\right]+V(x_i)\delta_{ij} \quad \text{if} \quad i=j.$$
[38] A. R. Edmonds, *Angular Momentum in Quantum Mechanics* (Princeton University Press, Princeton, 1960).
[39] G. G. Balint-Kurti, R. N. Dixon, and C. C. Marston, J. Chem. Soc., Faraday Trans. **86**, 1741 (1990).
[40] Á. Vibók and G. G. Balint-Kurti, J. Chem. Phys. **96**, 7615 (1992).
[41] C. C. Marston and G. G. Balint-Kurti, J. Chem. Phys. **91**, 3571 (1989).
[42] H. Tal-Ezer and R. Kosloff, J. Chem. Phys. **81**, 3967 (1984); R. Kosloff, J. Phys. Chem. **92**, 2087 (1988).
[43] K. A. Peterson, R. A. Kendall, and T. H. Dunning Jr., J. Chem. Phys. **99**, 1930 (1993).
[44] M. Bettendorff, R. J. Buenker, S. D. Peyerimhoff and J. Römelt, Z. Phys. A **304**, 125 (1982).
[45] G. A. Segal and K. Wolf, Chem. Phys. **56**, 321 (1981).
[46] T. H. Dunning, Jr., J. Chem. Phys. **65**, 3854 (1976).
[47] C. F. Bender and E. R. Davidson, J. Chem. Phys. **49**, 4989 (1968).
[48] R. A. Kendall, T. H. Dunning, Jr., and R. J. Harrison, J. Chem. Phys. **96**, 6796 (1992); D. E. Woon and T. H. Dunning, Jr., *ibid.* **98**, 1358 (1993).
[49] P. J. Knowles and H.-J. Werner, Chem. Phys. Lett. **115**, 259 (1985).
[50] H.-J. Werner and P. J. Knowles, J. Chem. Phys. **82**, 5053 (1985).
[51] H.-J. Werner and P. J. Knowles, J. Chem. Phys. **89**, 5803 (1988).
[52] P. J. Knowles and H.-J. Werner, Chem. Phys. Lett. **145**, 514 (1988).
[53] E. R. Davidson and D. W. Silver, Chem. Phys. Lett. **53**, 403 (1977).
[54] MOLPRO is a package of *ab initio* programs written by H.-J. Werner and P. J. Knowles, with contributions from R. D. Amos, A. Bernhardsson, A. Berning, P. Celani, D. L. Cooper, M. J. O. Deegan, A. J. Dobbyn, F. Eckert, C. Hampel, G. Hetzer, T. Korona, R. Lindh, A. W. Lloyd, S. J. McNicholas, F. R. Manby, W. Meyer, M. E. Mura, A. Nicklass, P. Palmieri, R. Pitzer, G. Rauhut, M. Schtz, H. Stoll, A. J. Stone, R. Tarroni, and T. Thorsteinsson, available from P. J. Knowles, Dept. of Chemistry, University of Birmingham, Birmingham BI5 2TT, U.K.
[55] S. F. Boys and F. Benardi, Mol. Phys. **19**, 553 (1970).
[56] K. P. Huber and G. Herzberg, *Molecular Spectra and Molecular Structure IV. Constants of Diatomic Molecules* (Van Nostrand, Princeton, 1979).
[57] R. J. LeRoy, J. Mol. Spectrosc. **194**, 189 (1999).
[58] C. E. Moore, *Atomic Energy Levels*, Natl. Stand. Ref. Data (U.S., Natl. Bur. Stand.) (1971).
[59] R. N. Zare, *Angular Momentum* (Wiley, New York, 1988).
[60] S. J. Singer and K. F. Freed, Adv. Chem. Phys. **61**, 1 (1985).